PRAMANA
— journal of
physics

Vol. 74, No. 2
February 2010
pp. 261–270

Structural stability and theoretical strength of Cu crystal under equal biaxial loading

JIAN-MIN ZHANG[1,*], ZHONG-LIANG LIN[1], YAN ZHANG[2] and VINCENT JI[2]
[1]College of Physics and Information Technology, Shaanxi Normal University, Xian 710062, Shaanxi, People's Republic of China
[2]ICMMO/LEMHE UMR CNRS 8182, Université Paris-Sud 11, 91405 Orsay Cedex, France
[*]Corresponding author. E-mail: jianm_zhang@yahoo.com

MS received 15 July 2009; revised 17 September 2009; accepted 24 September 2009

Abstract. Cu has been used extensively to replace Al as interconnects in ULSI and MEMS devices. However, because of the difference in the thermal expansion coefficients between the Cu film and the Si substrate, large biaxial stresses will be generated in the Cu film. Thus, the Cu film becomes unstable and even changes its morphologies which affects the device manufacturing yield and ultimate reliability. The structural stability and theoretical strength of Cu crystal under equal biaxial loading have been investigated by combining the MAEAM with Milstein-modified Born stability criteria. The results indicate that, under sufficient tension, there exists a stress-free BCC phase which is unstable and slips spontaneously to a stress-free metastable BCT phase by consuming internal energy. The stable region ranges from −15.131 GPa to 2.803 GPa in the theoretical strength or from −5.801% to 4.972% in the strain respectively.

Keywords. Structural stability; theoretical strength; equal biaxial loading; modified analytical embedded-atom method.

PACS Nos 73.61.At; 61.50.Ah; 05.70.Fh; 62.20.-x; 83.60.La

1. Introduction

Cu has been used extensively to replace Al as interconnects in ultra-large-scale integration (ULSI) circuits and micro-electromechanical systems (MEMS) [1]. The obvious advantage of using Cu stems from its lower resistivity ($\rho_{\mathrm{Cu}} = 1.67\ \mu\Omega$ cm, $\rho_{\mathrm{Al}} = 2.66\ \mu\Omega$ cm) and higher melting point ($T_{\mathrm{Cu}} = 1085^{\circ}$C, $T_{\mathrm{Al}} = 660^{\circ}$C). The former can lead to lower Joule heat as well as R–C delay, where R and C, respectively, represent the resistance and capacitance associated with interconnect architecture. The latter can result in higher electromigration resistance. However, because of the difference in the thermal expansion coefficients between the Cu film and the silicon substrate ($\alpha_{\mathrm{Cu}} = 17 \times 10^{-6}/^{\circ}$C, $\alpha_{\mathrm{Si}} = 3 \times 10^{-6}/^{\circ}$C), the larger Young's modulus ($E_{\mathrm{Cu}} = 129.8$ GPa, $E_{\mathrm{Al}} = 70.6$ GPa) and the large difference in thickness between the film and substrate ($h_{\mathrm{Si}}/h_{\mathrm{Cu}}$=400–500), large biaxial stresses will be generated

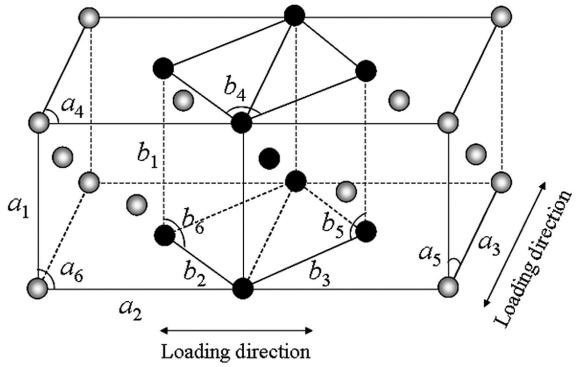

Figure 1. Two unit cells of initial FCC crystal.

in the Cu film during the thermal treatment process required for device fabrication and subsequent applications. When these stresses go beyond the theoretical strength, the Cu film becomes unstable and even changes its morphologies which are harmful to device manufacturing yield and ultimate circuit reliability. For example, large compressive stresses produce hillocks [2] on the film surface that lead to interlevel short circuiting between metallization layers. Large tensile stresses produce voids [3] in the film that locally reduce the film cross-section and current carrying capability of the interconnects. So it is necessary and important to study the structural stability and theoretical strength of Cu crystal under equal biaxial loading.

Although many experimental [4–7] and theoretical [8–16] methods have been used to investigate the structural stability and theoretical strength of various materials, most of them focus on the uniaxial [17] or hydrostatic [18] loading. In this paper, structural stability and theoretical strength of Cu crystal under equal biaxial loading along two edges of a unit cell are investigated by using the modified analytical embedded-atom method (MAEAM).

2. Computational methods

2.1 *Elastic theory*

Figure 1 shows schematically two unit cells in an FCC crystal subjected to equal biaxial stresses parallel to edges a_2 and a_3 and perpendicular to edge a_1. We use distinct edges a_1, a_2 and a_3 rather than the specific equivalence a_0 of the initial FCC crystal to represent a general case. Thus, the edges a_1, a_2 and a_3 will remain mutually perpendicular throughout the loading path (at least until failure occurs), i.e., the including angles a_4, a_5 and a_6 will maintain their initial values of $\pi/2$ and the initial FCC structure will change to the body-centred tetragonal (BCT) structure (see black atoms) with edges b_1, b_2 and b_3 ($b_1 \equiv a_1$, $b_2 \equiv b_3 \equiv (\sqrt{2}/2)a_2$) and the including angles b_4, b_5 and b_6 also maintaining the value $\pi/2$ as $a_2 \equiv a_3$.

The stress σ_α can be expressed as

$$\sigma_\alpha = \frac{d_\alpha}{V}\frac{\partial E_\mathrm{i}}{\partial a_\alpha}\bigg|_{\{a_\alpha\}}, \quad \alpha = 1,2,3,4,5,6 \tag{1}$$

where E_i is the internal energy per atom, $V = a_1 \times a_2 \times a_3/4$ is the current volume per atom, $d_\alpha = a_\alpha$ for the normal stresses σ_α ($\alpha = 1,2,3$) and $d_\alpha = 1$ for the shear stresses σ_α ($\alpha = 4,5,6$).

The elastic moduli $B_{\alpha\beta}$ can be expressed in terms of the second derivatives of the internal energy with respect to the lattice parameters a_α

$$B_{\alpha\beta} = \frac{\partial^2 E_\mathrm{i}}{\partial a_\alpha \partial a_\beta}\bigg|_{\{a_\alpha\}}, \quad \alpha,\beta = 1,2,3,4,5,6. \tag{2}$$

The necessary and sufficient conditions for the tetragonal lattice to be in stable equilibrium with respect to arbitrary homogeneous lattice strains are expressed in terms of the four independent moduli $B_{\alpha\beta}$ [8]

$$B_{12} > 0, \tag{3}$$

$$B_{23} > 0, \tag{4}$$

$$B_{22} - B_{23} > 0, \tag{5}$$

$$B_{11}(B_{22} + B_{23}) - 2B_{12}^2 > 0. \tag{6}$$

These relations also imply $B_{11} > 0$, $B_{22} > 0$. The theoretical strength is the value of the stress at which any one of the above four conditions is not satisfied.

2.2 *MAEAM*

In the MAEAM, the energy per atom E_i in the crystal is expressed as [19,20]

$$E_\mathrm{i} = F(\rho_i) + \frac{1}{2}\sum_{j(\neq i)} \phi(r_{ij}) + M(P_i), \tag{7}$$

$$\rho_i = \sum_{j(\neq i)} f(r_{ij}), \tag{8}$$

$$P_i = \sum_{j(\neq i)} f^2(r_{ij}), \tag{9}$$

where $F(\rho_i)$ is the energy to embed an atom i at site i with electron density ρ_i, which is given by a linear superposition of the spherically averaged atomic electron

density of other atoms $f(r_{ij})$, $\phi(r_{ij})$ is the interaction potential between atoms i and j and $M(P_i)$ is the modified term that describes the energy change due to the non-linear superposition of atomic electronic density P_i. r_{ij} is the distance of atom j from atom i at site i which is chosen as the origin of the coordinate system so that the subscript i in r_{ij} will be neglected in the following sections for convenience. For an FCC lattice subjected to uniform deformations, the vector $\vec{r}_j$ passing from the origin to the atom j can be written as

$$\vec{r}_j = \sum_{\alpha=1}^{3} r_{j\alpha}\hat{a}_\alpha = \frac{1}{2}\sum_{\alpha=1}^{3} l_{j\alpha}a_\alpha\hat{a}_\alpha, \tag{10}$$

where $\hat{a}_\alpha$ are unit vectors in the directions of the cell edges $a_\alpha(\alpha = 1, 2, 3)$. The reason for introducing the factors $\frac{1}{2}a_\alpha$ into (10) is to maintain $l_{j\alpha}$ as integers and subject to the condition that the sum $l_{j1}+l_{j2}+l_{j3}$ is even. The embedding function $F(\rho_i)$, pair potential $\phi(r_j)$, modified term $M(P_i)$ and atomic electron density $f(r_j)$ take the following forms [19,20]:

$$F(\rho_i) = -F_0\left[1 - n\ln\left(\frac{\rho_i}{\rho_e}\right)\right]\left(\frac{\rho_i}{\rho_e}\right)^n, \tag{11}$$

$$\phi(r_j) = k_0 + k_1\left(\frac{r_j}{r_{1e}}\right) + k_2\left(\frac{r_j}{r_{1e}}\right)^2 + k_3\left(\frac{r_j}{r_{1e}}\right)^6 + k_4\left(\frac{r_j}{r_{1e}}\right)^{-12} + k_5\left(\frac{r_j}{r_{1e}}\right)^{-1}, \tag{12}$$

$$M(P_i) = \gamma\left\{1 - \exp\left[-\left(\ln\left|\frac{P_i}{P_e}\right|\right)^2\right]\right\}, \tag{13}$$

$$f(r_j) = f_e\left(\frac{r_{1e}}{r_j}\right)^6, \tag{14}$$

where the subscript e indicates equilibrium state and r_{1e} is the first nearest-neighbour distance at equilibrium. In this paper, the cut-off distances of pair potential $\phi(r_j)$ and atomic electron density $f(r_j)$ are selected as $r_{ce} = r_{5e} + k_{ce}(r_{6e} - r_{5e})$ and $r_c = r_{6e} + 0.75(r_{7e} - r_{6e})$, respectively, where k_{ce} is the model parameter and r_{5e}, r_{6e} and r_{7e} are the fifth, sixth and seventh neighbour distance at equilibrium, respectively. F_0 and f_e can be calculated from [20]

$$F_0 = E_{\mathrm{c}} - E_{1\mathrm{f}}, \tag{15}$$

$$f_e = \sqrt{E_{\mathrm{c}}}/V_0, \tag{16}$$

where E_{c} is the cohesive energy and $E_{1\mathrm{f}}$ is the monovacancy formation energy and $V_0 = a_0^3/4$ is the initial atomic volume in FCC structure.

Table 1. The input physical parameters for Cu. a is in Å, $E_{\rm c}$ and $E_{1\rm f}$ are in eV and C_{ij} are in GPa.

a_0	$E_{\rm c}$	$E_{1\rm f}$	C_{11}	C_{12}	C_{44}
3.6147	3.49	1.17	169	122	75.3

Table 2. The calculated parameters for Cu, n and k_{ce} are dimensionless, F_0, γ and k_i are in eV.

n	k_{ce}	F_0	γ	k_0	k_1	k_2	k_3	k_4	k_5
0.60	0.3	2.32	0.00316257	1.499487	−0.650171	0.097645	−0.000056	0.098837	−1.178326

The remaining model parameters can be calculated from the physical parameters [20], the lattice constant a_0, cohesive energy $E_{\rm c}$, monovacancy formation energy $E_{1\rm f}$ and elastic constants C_{11}, C_{12} and C_{44}. The physical parameters used in this paper and the calculated model parameters for Cu are listed in tables 1 and 2, respectively.

Based on the symmetry of the tetragonal crystal and using (1)–(2), and (7)–(16) we get

$$\sigma_\alpha = \frac{1}{V}\left[F'(\rho)\sum_j \frac{(r_{j\alpha})^2}{r_j} f'(r_j) + \frac{1}{2}\sum_j \frac{(r_{j\alpha})^2}{r_j}\phi'(r_j) + 2M'(P)\sum_j \frac{(r_{j\alpha})^2}{r_j} f(r_j) f'(r_j)\right]\left(\frac{a_0}{a_\alpha}\right), \tag{17}$$

$$\begin{aligned} B_{11} = \Bigg\{ & F''(\rho)\left(\sum_j \frac{(r_{j1})^2}{r_j} f'(r_j)\right)^2 + F'(\rho)\sum_j \left(\frac{(r_{j1})^2}{r_j}\right)^2 \\ & \times \left(f''(r_j) - \frac{f'(r_j)}{r_j}\right) + F'(\rho)\sum_j \frac{(r_{j1})^2}{r_j} f'(r_j) \\ & + \frac{1}{2}\sum_j \left(\frac{(r_{j1})^2}{r_j}\right)^2 \left(\phi''(r_j) - \frac{\phi'(r_j)}{r_j}\right) \\ & + \frac{1}{2}\sum_j \frac{(r_{j1})^2}{r_j}\phi'(r_j) + 4M''(P)\left[\sum_j f(r_j) f'(r_j)\frac{(r_{j1})^2}{r_j}\right]^2 \\ & + 2M'(P)\sum_j \left(\frac{(r_{j1})^2}{r_j}\right)^2 \left(f'(r_j)^2 + f(r_j) f''(r_j) - \frac{f'(r_j) f(r_j)}{r_j}\right) \\ & + 2M'(P)\sum_j \frac{(r_{j1})^2}{r_j} f(r_j) f'(r_j)\Bigg\}\left(\frac{1}{a_1}\right)^2, \end{aligned} \tag{18}$$

$$B_{12} = \Bigg\{ F''(\rho) \left[\sum_j \frac{(r_{j1})^2}{r_j} f'(r_j) \right] \left[\sum_m \frac{(r_{j2})^2}{r_j} f'(r_j) \right] + F'(\rho) \sum_j \left(\frac{r_{j1} r_{j2}}{r_j} \right)^2 \left(f''(r_j) - \frac{f'(r_j)}{r_j} \right) + \frac{1}{2} \sum_j \left(\frac{r_{j1} r_{j2}}{r_j} \right)^2 \left(\phi''(r_j) - \frac{\phi'(r_j)}{r_j} \right) + 4M''(P) \left[\sum_j \frac{(r_{j1})^2}{r_j} f(r_j) f'(r_j) \right] \left[\sum_j \frac{(r_{j2})^2}{r_j} f(r_j) f'(r_j) \right] + 2M'(P) \sum_j \left(\frac{r_{j1} r_{j2}}{r_j} \right)^2 \left(f'(r_j)^2 + f(r_j) f''(r_j) - \frac{f(r_j) f'(r_j)}{r_j} \right) \Bigg\} \left(\frac{1}{a_1 a_2} \right), \tag{19}$$

$$B_{44} = \Bigg\{ F'(\rho) \sum_j \left(\frac{r_{j2} r_{j3}}{r_j} \right)^2 \left(f''(r_j) - \frac{f'(r_j)}{r_j} \right) + \frac{1}{2} \sum_j \left(\frac{r_{j2} r_{j3}}{r_j} \right)^2 \times \left(\phi''(r_j) - \frac{\phi'(r_j)}{r_j} \right) + 2M'(P) \sum_j \left(\frac{r_{j2} r_{j3}}{r_j} \right)^2 \times \left(f'(r_j)^2 + f(r_j) f''(r_j) - \frac{f(r_j) f'(r_j)}{r_j} \right) \Bigg\}. \tag{20}$$

The remaining $B_{\alpha\beta}$ can be obtained by switching subscripts in the above equations. For example, to find B_{22}, r_{j1} and a_1 are changed to r_{j2} and a_2 in (18); for B_{23}, r_{j1} and a_1 are changed to r_{j3} and a_3 in (19); and for $B_{55} = B_{66}$, r_{j3} and a_3 are changed to r_{j1} and a_1 in (20).

2.3 *Simulation procedures*

The procedures for determining the variation of the internal energy per atom $E(= E_{\mathrm{i}})$, the normal stress σ_α and the elastic moduli $B_{\alpha\beta}$ with the values of the edges a_α, follow these processes:

(1) Elongate (or contract) the edge a_2 by a small amount Δa_2 to $a_2 + \Delta a_2$ and maintain $a_2 \equiv a_3$;
(2) Calculate the value of the edge a_1 by allowing the crystal to relax to the state of $\sigma_1 = 0$;

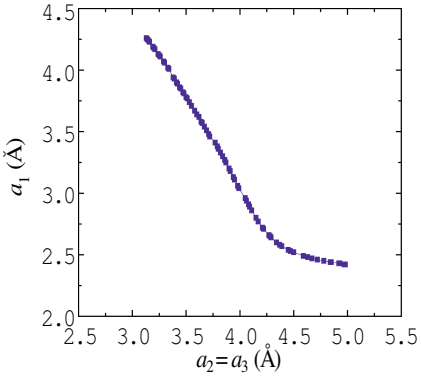

Figure 2. Variation of a_1 with a_2.

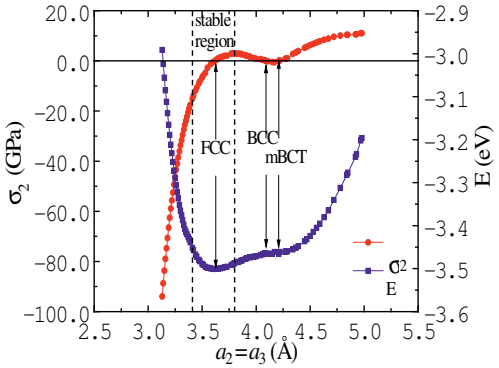

Figure 3. Variation of E and σ_2 with a_2.

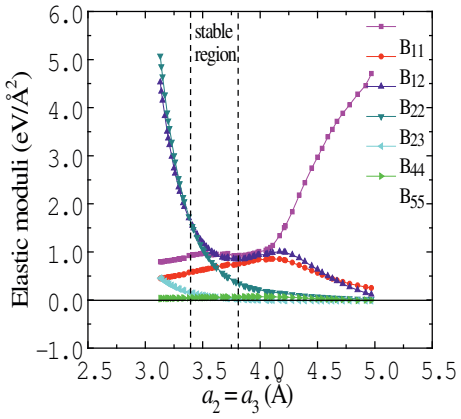

Figure 4. Variation of elastic moduli with a_2.

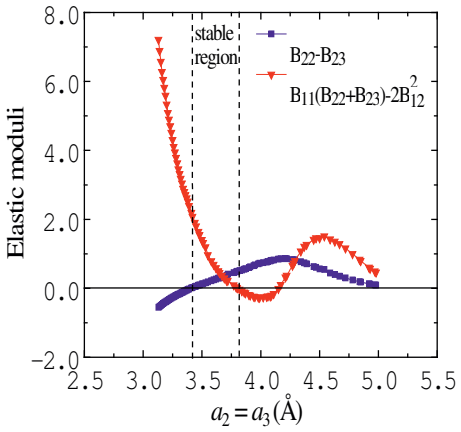

Figure 5. Variation of the combinated elastic moduli with a_2.

(3) Use (7)–(20) to calculate the internal energy per atom E, the normal stresses σ_2 and σ_3 and the elastic moduli $B_{\alpha\beta}$;
(4) Repeat the above processes many times until a sufficient deformation is achieved.

3. Results and discussions

The calculated lattice parameter a_1, the energy per atom E and the normal stress $\sigma_2(\equiv \sigma_3)$, the six independent elastic moduli B_{11}, B_{12}, B_{22}, B_{23}, B_{44} and B_{55}, and their combinations $B_{22} - B_{23}$ and $B_{11}(B_{22} + B_{23}) - 2B_{12}^2$ related to the stability criteria are shown in figures 2–5 respectively, as a function of edge $a_2(\equiv a_3)$. From figure 2 we know that, as is predicted, the lattice parameter a_1 decreases with increasing $a_2(\equiv a_3)$.

Figure 3 shows that in the beginning the internal energy per atom E of the crystal achieves the lowest value of -3.501 eV at $a_2 = 3.62$ Å corresponding to the stress-free equilibrium FCC structure. With increasing lattice parameter $a_2(\equiv a_3)$, the internal energy per atom E increases firstly to the local maximum value of -3.465 eV at $a_2 = 4.09$ Å, then decreases slightly to the local minimum value of -3.466 eV at $a_2 = 4.21$ Å and then increases monotonously with further tension. There is an unconventional behaviour in the corresponding region for the stress. The stress $\sigma_2(\equiv \sigma_3)$ passes through zero at two other values of lattice parameter, $a_2 = 4.09$ Å and $a_2 = 4.21$ Å. These two points correspond to a local maximum and a local minimum of the internal energy of the crystal, respectively. In detail, as the FCC crystal is subjected to unconstrained tension, the normal stress $\sigma_2(\equiv \sigma_3)$ initially increases, then decreases, passing through zero and becoming negative at $a_2 = 4.09$ Å and then increases passing through zero and becoming positive again at $a_2 = 4.21$ Å. In compression region, a conventional behaviour is obtained. That is, by decreasing the lattice parameter $a_2(\equiv a_3)$, the normal stress $\sigma_2(\equiv \sigma_3)$ decreases monotonously with a monotonous increase in the internal energy E.

As mentioned above, when an FCC crystal is subjected to equal biaxial stresses along the edges a_2 and a_3, the homogeneously deformed crystal structure can be termed as a BCT structure (shown as black atoms in figure 1). The point of $a_2 = a_3 = 4.09$ Å and correspondingly $a_1 = 2.89$ Å, makes $b_1 \equiv a_1 = 2.89$ Å and $b_2 \equiv b_3 \equiv \frac{\sqrt{2}}{2}a_2 = \frac{\sqrt{2}}{2} \times 4.09 \approx 2.892$ Å, nearly satisfies the relation $b_1 = b_2 = b_3$. Thus this point corresponds to a BCC phase (specified by BCC in figure 3). This was also obtained by Milstein *et al* with central-force Morse potential calculation and termed as Bain phase transformation under unaxial loading. Since the BCC phase corresponds to the local maximum internal energy $E_{\mathrm{BCC}} = -3.465$ eV, it is unstable and would slip spontaneously into a metastable BCT phase (specified by mBCT in figure 3) with a local minimum internal energy $E_{\mathrm{mBCT}} = -3.466$ eV at $a_2 = a_3 = 4.21$ Å. This process is termed as a spontaneous process, because it is driven by decreasing internal energy and so a small negative (compressive) stress is sensed in figure 3. The initial FCC phase corresponds to the lowest internal energy and is evidently the most stable structure. This is in correspondence with the actual behaviour of pure Cu which exists in the FCC phase.

In figure 5, the units of $B_{22} - B_{23}$ and $B_{11}(B_{22} + B_{23}) - 2B_{12}^2$ are eV/Å^2 and (eV/Å^2)^2, respectively. It is found that the failure occurs firstly in compression when the condition $B_{22} - B_{23} > 0$ is violated at the lattice parameter $a_2 = a_3 = 3.41$ Å where the lattice cannot support an additional compressive loading. Beyond this point, a further decrease in lattice parameter $a_2(\equiv a_3)$ leads to a monotonous decrease in the stress $\sigma_2(\equiv \sigma_3)$ as shown in figure 3. Correspondingly, failure occurs in tension region while $B_{11}(B_{22} + B_{23}) - 2B_{12}^2 > 0$ is violated at the lattice parameter about $a_2 = a_3 = 3.80$ Å where the lattice cannot accommodate enough stress. Beyond this point, a further increase in lattice parameter $a_2(\equiv a_3)$ results in a decrease rather than an increase in tension stress $\sigma_2(\equiv \sigma_3)$ as shown in figure 3. At these two points, the applied stress $\sigma_2(\equiv \sigma_3)$ is equal to -15.131 GPa and 2.803 GPa, respectively. The stable region determined (3.41 Å $< a_2 <$ 3.80 Å, between two vertical dashed lines in figures 3–5) satisfies the remaining two stability criteria $B_{12} > 0$ and $B_{23} > 0$ as can be seen in figure 4. Furthermore, the relations $B_{11} = B_{22}$, $B_{12} = B_{23}$ and $B_{44} = B_{55}$ are satisfied at $a_1 = a_2 = a_3 = 3.62$ Å for

FCC structure. It is worth mentioning that although figures 4 and 5 show that the other region 4.17 Å $< a_2 <$ 5.0 Å also satisfies the stability criteria (3)–(6), as can be seen in figure 3, the internal energy per atom E corresponding to this region is obviously higher than that in the region 3.41 Å $< a_2 <$ 3.80 Å. So the other region 4.17 Å $< a_2 <$5.0 Å is not a stable region but a metastable region. Thus, for the Cu crystal under equal biaxial loading along the edges a_2 and a_3, the stability of the lattice ranges from $a_2 = a_3 =$ 3.41 Å to $a_2 = a_3 =$ 3.80 Å and the corresponding strain ranges from −5.801% to 4.972%; the theoretical strength is −15.131 GPa in compression and 2.803 GPa in tension.

4. Conclusions

The present paper studies the structural stability and theoretical strength of Cu crystal under equal biaxial loading by the MAEAM according to Milstein-modified Born stability criteria. The results are listed as follows:

(1) The FCC phase has the lowest energy of −3.501 eV and this is the most stable phase, which is in agreement with the actual behaviour of pure Cu existed in the FCC phase, in spite of a stress-free BCC phase with the local maximum energy of −3.465 eV appeared in tensile region would slip spontaneously (driven by consuming internal energy so a negative (compressive) stress is sensed) into the near neighbour stress-free mBCT phase with a local minimum energy of −3.466 eV.
(2) The stable region of Cu crystal is determined by $B_{22} - B_{23} > 0$ in compression and $B_{11}(B_{22} + B_{23}) - 2B_{12}^2 > 0$ in tension.
(3) The stable region is determined for the theoretical strength ranging from −15.131 GPa in compression to 2.803 GPa in tension and the corresponding strain ranges from −5.801% to 4.972%.

Acknowledgements

The authors would like to acknowledge the State Key Development for Basic Research of China (Grant No. 2004CB619302) for providing financial support for this research.

References

[1] S P Mararka, *Mater. Sci. Eng.* **R19**, 87 (1997)
[2] P Chaudhair, *J. Appl. Phys.* **45**, 4339 (1974)
[3] P Børgesen, J K Lee, R Gleixner and C Y Li, *Appl. Phys. Lett.* **60**, 1706 (1992)
[4] S S Brenner, *J. Appl. Phys.* **27**, 1484 (1956)
[5] H Kobayashi and Y Hiki, *Phys. Rev.* **B7**, 594 (1973)
[6] C R Krenn, D Roundy, M L Cohen, D C Chrzan and J W Morris Jr, *Phys. Rev.* **B65**, 134111 (2002)
[7] T Davenport, L Zhou and J Trivisonno, *Phys. Rev.* **B59**, 3421 (1999)

[8] F Milstein, *Phys. Rev.* **B3**, 1130 (1970)
[9] K Huang, F Milstein and J A J Baldwin, *Phys. Rev.* **B10**, 3635 (1974)
[10] C V Pandya, P R Vyas, T C Pandya, N Ranil and V B Gohel, *Physica* **B307**, 138 (2001)
[11] F Milstein and S Chantasiriwan, *Phys. Rev.* **B58**, 6006 (1998)
[12] F Ma and K W Xu, *Solid State Commun.* **140**, 487 (2006)
[13] Y Mishin, M J Mehl and D A Papaconstantopoulos, *Acta Mater.* **53**, 4029 (2005)
[14] J H Shim, H J Lee and B D Wirth, *J. Nucl. Mater.* **351**, 56 (2006)
[15] D M Clatterbuck, D C Chrzan and J W Morris Jr, *Acta Mater.* **51**, 2271 (2003)
[16] M Černý and J Pokluda, *J. Alloys Compounds* **378**, 159 (2004)
[17] J M Zhang, Y Yang, K W Xu and V Ji, *Can. J. Phys.* **86**, 935 (2008)
[18] H T Li, J M Zhang and K W Xu, *Mater. Sci. Eng.* **A485**, 627 (2008)
[19] W Y Hu, X L Shu and B W Zhang, *Comput. Mater. Sci.* **23**, 175 (2002)
[20] F Fang, X L Shu, H Q Deng, W Y Hu and M Zhu, *Mater. Sci. Eng.* **A355**, 357 (2003)